Supporting Information

Niedermayer et al. 10.1073/pnas.1121381109

SI Text

Theoretical Analysis of Different Interruption Mechanisms. It is well-established that each actin protomer can attain several nucleotide states depending on the occupation of its nucleotide binding pocket. Our experiments demonstrate, however, that the interruptions of the depolymerization are not related to these nucleotide states because they occur for filaments assembled from ATP-actin, ADP/P_i-actin as well as ADP-actin. Therefore, our theoretical analysis proceeds in several steps.

First, we ignore the details of ATP hydrolysis and combine the different nucleotide states into a single, coarse-grained protomer state, called "state 1" in the following. The interruptions, on the other hand, are taken to arise from another, transformed "state 2" at the barbed end that is characterized by a very small dissociation rate at this end.

Second, we study several different mechanisms for the transitions of protomer state 1 to protomer state 2: a variety of transitions that give rise to exponential distributions such as a global structural transformation of the whole filament or copolymerization of two types of actin monomers—vectorial processes related to the nucleation and growth of a filament segment consisting of state 2 and protomer transitions at random filament sites. In all cases, we derive relatively simple analytical expressions for the corresponding cumulative distributions and confirm these expressions by extensive simulations.

Third, we refine our theory and incorporate the different nucleotide states into it. As a result, the functional form of the cumulative distribution is found to undergo relatively small changes that do not affect the conclusions of the coarse-grained description.

Fourth, we derive the cumulative distribution for random transitions that occur only for the fluorescently labeled protomers. We show that the transition rate becomes proportional to the fraction of the labeled protomers in agreement with the experimental observations, provided the transitions occur at single labeled protomers.

Finally, we consider the depolymerization of filaments that have been copolymerized from G-actin monomers and preformed actin dimers. The depolymerization process is now interrupted both by preformed and by photo-induced dimers. The corresponding cumulative distribution contains an exponential time dependence arising from the preformed dimers as well as a Gaussian time dependence arising from the photo-induced dimers.

Transition mechanisms that give rise to exponential distributions. In the simplest case, the filament as a whole undergoes a transition from state 1 to state 2, or the transition occurs randomly at the tip, either caused by contacts or by a contaminating capping protein. Such a change from the shrinking to the no-shrinking phase is caused by a single stochastic transition that implies a probability density $\Phi(\tau) = \omega \exp\{-\omega\tau\}$ and a cumulative distribution

$$P(t) \equiv \int_0^t d\tau \Phi(\tau) = 1 - \exp\{-\omega t\}. \qquad \textbf{[S1]}$$

In the second case, the probability that a protomer is in state 2, is time independent and constant along the filament. This situation could arise, for instance, from a transition process that is coupled to polymerization: As monomers are incorporated into the filament, they are directly converted into state 2 with a certain probability Q. Alternatively, one can interpret Q as the probability that a protomer is anchored to the coverslip surface. Thus, tethering of a certain fraction of protomers to this surface would also lead to an exponential distribution, corresponding to the red curves in Fig. 2 *B* and *Cc*.

The depolymerization of the filament consists of many stochastic dissociation events. However, the length fluctuations are small compared to the total length of the filaments. In consequence, the stochasticity of the depolymerization process is small compared to the stochasticity arising from the transformed state-2-protomers along the filament as confirmed by stochastic simulations employing the Gillespie algorithm (1); see Fig. S1.

The probability that a filament is in the initial shrinking phase is given by $1 - P(t)$. This phase is terminated in an abrupt manner, when a protomer in state 2 reaches the barbed end. The rate at which such an event occurs is given by the probability Q that the penultimate protomer is in state 2 times the depolymerization velocity v_{dep}. Therefore, the time evolution of $P(t)$ is governed by

$$\frac{\partial}{\partial t}(1 - P(t)) = -Qv_{\mathrm{dep}}(1 - P(t)) \qquad \textbf{[S2]}$$

As a first approximation, the depolymerization velocity v_{dep} is taken to be time independent. With the initial condition $P(0) = 0$, the solution of Eq. **S2** is given by

$$P(t) = 1 - \exp\{-\omega t\}, \quad \text{with } \omega = Qv_{\mathrm{dep}}. \qquad \textbf{[S3]}$$

Experimentally, we found that the average value $\langle\tau\rangle$ of the duration of the first shrinking phase is of the order of 10^3 s, which would imply that the transition rate ω is about 10^{-3}/s, and that Q is of the order of 10^{-4} for $v_{\mathrm{dep}} \simeq 5$/s.

Vectorial process. Starting from the seed at the pointed end, which represents the oldest filament segment, protomers successively undergo transitions from state 1 to 2. The shrinking phase ends when a protomer in state 2 reaches the barbed end. Thus, for this vectorial process, all protomers have undergone the transition to state 2 in the no-shrinking phase.

Thousands of subsequent and independent transitions from state 1 to 2 and association/dissociation events occur before the shrinking phase ends. As a consequence, the fluctuations in τ are expected to be small compared to $\langle\tau\rangle$. However, because the fluctuations from both sources (transitions and association/dissociation events) are comparable in size, we must take all stochastic processes into account: association of monomers during the growth phase with rate ω_{on}, dissociation of protomers during the growth phase with rate $\omega_{\mathrm{off}}^{\mathrm{el}}$, dissociation of protomers during the shrinking phase possibly with different rate ω_{off}, as well as transitions from state 1 to state 2 with rate ω at the boundary between the shrinking state-1-segment and the growing state-2-segment of the filament.

It turns out that an excellent approximation for the cumulative distribution of such a vectorial process is given by

$$P(t) = \Phi\left(\frac{t - \mu}{\sigma}\right), \qquad \textbf{[S4]}$$

with the standard normal integral

$$\Phi(x) \equiv \frac{1}{\sqrt{2\pi}} \int_{-\infty}^{x} dy e^{-y^2/2} \qquad \textbf{[S5]}$$

and the two parameters

$$\mu = \frac{\omega_{on} - \omega_{off}^{el} - \omega}{\omega_{off} + \omega} t_{pol} \quad \textbf{[S6]}$$

as well as

$$\sigma^2 = \frac{2\omega_{on}}{(\omega_{off} + \omega)^2} t_{pol}, \quad \textbf{[S7]}$$

where t_{pol} denotes the duration of the polymerization phase. We have confirmed the validity of this approximation by stochastic simulations; see Fig. S1.

Protomer Transitions at Random Sites. In a random process, all protomers can independently undergo a transition from state 1 to state 2 once they are incorporated into the filament. In a typical experiment, a few thousand protomers dissociate, before a single protomer in state 2 appears at the barbed end and blocks the depolymerization process. Thus, the order of magnitude of the transition rate ω can be estimated from the average duration $\langle\tau\rangle$ via $10^3\omega \simeq 1/\langle\tau\rangle$ giving $\omega \simeq 10^{-6}$/s. Compared to the association/dissociation events, the rare protomer transitions have a much bigger stochastic effect on the system as confirmed by stochastic simulations; see Fig. S1.

As before, we start with a time-independent depolymerization velocity v_{dep}. In analogy to Eq. **S2**, the time evolution of the probability $1 - P(t)$ that a filament is in the initial shrinking phase is governed by

$$\frac{\partial}{\partial t}(1 - P(t)) = -Q(t) v_{dep}(1 - P(t)), \quad \textbf{[S8]}$$

where $Q(t)$ is the time-dependent probability that the protomer at the penultimate position is in state 2. In a random process, $Q(t)$ is solely determined by the protomer "age," i.e., the time that has elapsed since this protomer has been incorporated into the filament. Assuming both a constant polymerization velocity v_{pol} and a constant depolymerization velocity v_{dep}, the age of the protomer at the penultimate position is given by $a(t) = (1 + v_{dep}/v_{pol})t$, which implies

$$Q(t) = 1 - \exp\{-\omega(1 + v_{dep}/v_{pol})t\} \approx \omega(1 + v_{dep}/v_{pol})t \quad \textbf{[S9]}$$

for $v_{dep} < v_{pol}$ and $\omega t \ll 1$. Inserting Eq. **S9** into Eq. **S8**, and using the initial condition $P(0) = 0$, we obtain

$$P(t) = 1 - \exp\left\{-\frac{\omega v_{dep}(1 + v_{dep}/v_{pol})}{2} t^2\right\}. \quad \textbf{[S10]}$$

This distribution is qualitatively different from both the exponential distributions in Eqs. **S1** and **S3** and the standard normal integral in Eq. **S4**. It has a sigmoidal shape and increases only slowly.

Effect of hydrolysis. If the filament is grown from ATP-actin, hydrolysis increases the depolymerization velocity $v_{dep}(t)$ (see Fig. 1*H* of the main text) and thus alters the cumulative distribution function $P(t)$. In ref. 2 we have analyzed the time dependence of $v_{dep}(t)$ in detail. After some computation, the length as a function of time $L(t)$ is found to be implicitly described by the differential equation

$$\frac{\partial L(t)}{\partial t} = \frac{-1}{\frac{1}{v_D} + (\frac{1}{v_P} - \frac{1}{v_D})\exp\{-\omega_r(t + t_{pol} - L(t)/v_{pol})\}}, \quad \textbf{[S11]}$$

where $v_P \simeq 1.5$/s is the effective depolymerization velocity of ADP-Pi-actin and $v_D \simeq 6.2$/s is the depolymerization velocity of ADP-actin. Both the duration t_{pol} and the velocity v_{pol} of the polymerization process represent control parameters that may vary for different experiments. Using the time-dependent depolymerization velocity $v_{dep}(t) = -\partial L(t)/\partial t$, Eq. **S10** is generalized to

$$P(t) = 1 - \exp\left\{-\int_0^t dt' v_{dep}(t') Q(t')\right\}, \quad \textbf{[S12]}$$

where

$$Q(t) = 1 - \exp\{-\omega a(t)\} \quad \textbf{[S13]}$$

is the probability that the penultimate protomer is in state 2 and

$$a(t) = t + t_{pol} - L(t)/v_{pol}. \quad \textbf{[S14]}$$

denotes the protomer age. For realistic values of the parameters, the relation **[S12–S14]**, that incorporate the effects of ATP hydrolysis, give qualitatively the same flat and sigmoidal distribution as the simple eEq. **S10**;see Fig. S2.

Transitions of single, fluorescently labeled protomers. It turns out experimentally that the transition rate ω is proportional to the labeling fraction X_{fl}; see Fig. 3*A* of the main text. In addition, nonlabeled filament segments seem to depolymerize completely, without any interruptions; see Fig. 3*D* of the main text. From these findings, we conclude that only labeled protomers are able to undergo the transition and that a transition involves only a single labeled protomer. A putative interaction between two such protomers, for instance, would lead to a quadratic dependence of ω on the labeling fraction X_{fl}.

In consequence, we can interpret $\omega \equiv X_{fl}\omega_{fl}$ as an effective rate, where the transition rate ω_{fl} of a labeled protomer is of the order of 10^{-5}/s. In analogy to Eq. **S9**, we have

$$\begin{aligned} Q(t) &= X_{fl}(1 - \exp\{-\omega_{fl}(1 + v_{dep}/v_{pol})t\}) \\ &\approx X_{fl}\omega_{fl}(1 + v_{dep}/v_{pol})t, \end{aligned} \quad \textbf{[S15]}$$

because $\omega_{fl}t \ll 1$. The functional forms of Eq. **S9** and Eq. **S13** remain unaltered, but the protomer transition rate ω now has a more precise molecular interpretation.

Incorporation of preformed dimers. To study the pauses caused by preformed covalent actin dimers, we copolymerized actin monomers with such preformed dimers. In this case, the pauses occurring during depolymerization are caused both by preformed and photo-induced dimers. On the lines of the previous sections, one can calculate the cumulative distribution $P(t)$ for their first occurrence. The time-dependent probability $Q(t)$ that a dimer is at the penultimate position is given by

$$\begin{aligned} Q(t) &= 1 - (1 - Q_0)\exp\{-\omega(1 + v_{dep}/v_{pol})t\} \approx Q_0 \\ &\quad + \omega(1 + v_{dep}/v_{pol})t, \end{aligned} \quad \textbf{[S16]}$$

where Q_0 is the mole fraction of dimers initially present in the filament, and ω is the transition rate as defined before. The approximated expression holds for $Q_0 \ll 1$, $v_{dep} < v_{pol}$ and $\omega t \ll 1$. Insertion into Eq. **S8** and integration leads to

$$P(t) = 1 - \exp\{-v_{dep}Q_0 t - v_{dep}\omega(1 + v_{dep}/v_{pol})t^2/2\}. \quad \textbf{[S17]}$$

Variation of Illumination. We varied the intensity of the illumination to investigate its influence on the transition. The results, shown in Fig. 3*B*, were obtained in the following way. We performed epifluorescence microscopy with a Lumen Dynamics X-Cite 120Q light source and a Semrock Brightline 482/35 filter. This setup ensures a very flat spectral density for wavelengths between 464.5 and 499.5 nm. This range of wavelengths contains 93% of the light intensity. To determine the light intensity in the sample, we separately measured the power entering the rear of the objective using a laser power meter (Coherent, Fielm MAXII-TO). Assuming that there is almost no loss in the objective, in the microscope oil, and in the coverslip, this power corresponds to the overall power illuminating the sample. All light is focused by the objective to a spot with a diameter of 150 μm, corresponding to an illuminated area of 0.0177 mm^2. For the four datasets shown in Fig. 3*B*, we used three different power settings of the light source: 1.80 mW, 0.66 mW, and 0.30 mW, corresponding to an illumination intensity of 102 mW/mm^2, 37 mW/mm^2, and 17 mW/mm^2, respectively. Apart from the lowest magenta curve in Fig. 3*B*, the filaments were illuminated every 20 s with an exposure time of 0.5 s, leading to an average intensity of 2.54 mW/mm^2, 0.93 mW/mm^2, and 0.42 mW/mm^2, respectively. For the lowest magenta curve, the average intensity was further decreased to 0.21 mW/mm^2 by doubling the interval to 40 s, and keeping the illumination intensity at 17 mW/mm^2.

Copolymerization of Actin Monomers and Preformed Actin Dimers. As shown in Fig. 4*B*, we also studied the depolymerization of individual filaments that were copolymerized from G-actin monomers and preformed actin dimers. Because we were interested in the pauses caused by the preformed dimers and not in those caused by the photo-induced dimers, we used a low illumination intensity to observe the filaments. For these illumination conditions, we first determined the transition rate ω by studying the depolymerization of filaments grown from G-actin monomers with labeling fraction $X_{fl} = 0.1$ in the absence of preformed dimers. As before, we identified those filaments that did not shrink at all. We excluded this small nondepolymerizing fraction of filaments and applied the Kaplan–Meier-estimator to obtain the empirical cumulative distribution function. This distribution, which corresponds to the blue multistep function in Fig. 4*B*, was then fitted to Eq. (1), from which we obtained the transition rate $\omega = 4.9 \times 10^{-7}/s$.

Next, we studied the depolymerization of filaments that were copolymerized from G-actin monomers, again with labeling fraction $X_{fl} = 0.1$, and preformed dimers. The molar concentration of G-actin was kept close to 2 μM (it varied between 2 and 2.1 μM) whereas the molar concentration of the preformed dimers was taken to be 2, 4, and 8 nM. In this case, the data analysis was performed as follows. First, we applied the Kaplan–Meier-estimator to the experimental data to obtain the experimental cumulative distribution function $P_{exp}(t)$. These data included a certain fraction R_0 of nondepolymerizing filaments. The multistep function $P_{exp}(t)$ was then fitted to the distribution $R_0 + (1 - R_0)P(t)$, where the cumulative distribution function $P(t)$ is now given by Eq. **S17** in the *SI Text*. The latter distribution function describes the combined effect of preformed and photo-induced dimers and depends on the mole fraction Q_0 of preformed dimers, initially present in the filaments. In this analysis, we used both R_0 and Q_0 as fit parameters. The reddish data shown in Fig. 4*B* represent the empirical cumulative distribution functions as given by $(P_{exp}(t) - R_0)/(1 - R_0)$ together with the fitted cumulative distribution functions $P(t)$ as in Eq. **S17**. As expected, we found that the mole fraction Q_0 of dimers initially present in the filament is proportional to the mole fraction of preformed dimers in the polymerization solution. Interestingly, the ratio of these mole fractions is about 0.5 indicating that the association rate of the dimers is about half the association rate of the monomers.

Western Blots of Preformed and Photo-Induced Actin Dimers. ***Preformed covalent dimers.*** Cross-linked actin dimers were formed in F-actin by N,N′-p- phenylenedimaleimide, which forms a covalent bond between Cys-374 of one protomer and Lys-191 of an adjacent protomer. After depolymerization of the filaments, the resulting concentration of dimers was determined by SDS/PAGE gel electrophoresis. These preformed dimers were used for comparison and calibration in the Western blots (see Fig. 4*A*) and were copolymerized with labeled G-actin. The resulting cumulative distribution functions P are shown in Fig. 4*B* for several concentrations of preformed dimers.

Fraction of photo-induced dimers by Western blots. F-actin solutions were placed in a quartz cuvette and exposed to collimated light from the Xcite lamp of the microscope, with an illumination intensity of 0.04 mW/mm^2. The dimer-to-monomer ratio in these samples was determined from the Western blots, using the "Gels" analysis function in ImageJ, and using the preformed dimer solutions for calibration. No dimers were found in the unexposed nonlabeled actin sample. The dimer concentrations measured in the samples of labeled-actin were consistent with the transition rates ω_{fl} determined from the cumulative distributions P of initial shrinking phase durations: a dimer-to-monomer ratio of approximately 3×10^{-3} was measured in F-actin with 41.6% Alexa488 exposed for 2.5 h (sample shown in Fig. 4*A* of the main text), and a ratio of approximately 4×10^{-4} was measured in F-actin with 10% Alexa488 exposed for 1 h.

Dimerization of G-actin. Photo-induced dimerization was also observed in illuminated solutions of labeled G-actin; see Fig. S4. In contrast to F-actin, where the protomers are in permanent contact with their neighbors, monomers in G-actin buffer come into contact via collisions, with a frequency that depends quadratically on their concentration. Based on our results for 52 μM G-actin (see Fig. S4), the dimerization rate in 1 μM G-actin is estimated to be about 30 times smaller than for F-actin, under identical illumination conditions. In conventional microscopy experiments, the relative importance of photo-induced G-actin dimerization is further reduced by the diffusive motion of monomers in and out of the illuminated region, hereby receiving less light than the protomers within the filaments. In our microfluidics experiments, photo-induced dimerization of G-actin is certainly irrelevant, because filaments elongate from fresh G-actin that constantly entered the flow cell without being previously illuminated. In fact, if G-actin dimers were present and incorporated into the filaments, they would affect the cumulative distribution $P = P(t)$ in the same way as the preformed dimers: this distribution would no longer have a sigmoidal shape as in Fig. 3 but rather a convex shape as the three upper curves in Fig. 4*B*.

1. Gillespie D (1977) Exact stochastic simulation of coupled chemical reactions. *J Phys Chem* 81: 2340–2361.

2. Jégou A, Niedermayer T, Orbán J, Didry D, Lipowsky R, et al. (2011) Individual actin laments in a microfluidic flow reveal the mechanism of ATP hydrolysis and give insight into the properties of prolin. *PLoS Biol* 9: e1001161.

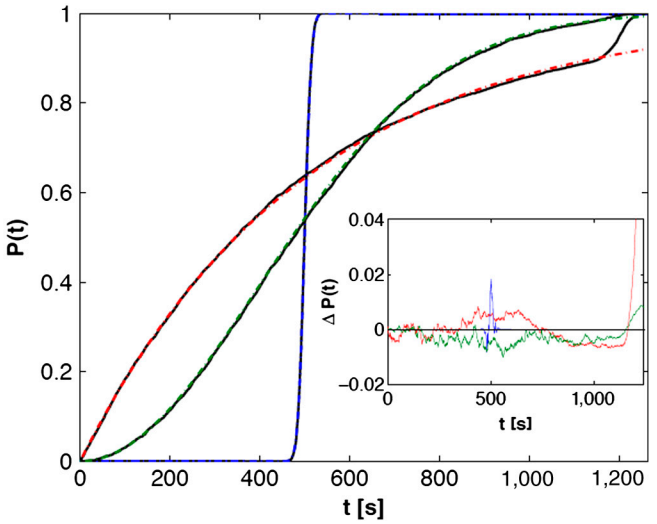

Fig. S1. Analytical results are in very good agreement with stochastic simulations. The cumulative distribution functions P versus time t for three different transition mechanisms: transitions coupled to polymerization (red/black line), vectorial transitions (blue/black line), and random transitions (green/black line). The red, blue, and green lines correspond to the analytical results in Eqs. **S3**, **S4**, and **S10**, respectively. The black lines represent the corresponding results of stochastic simulations using the Gillespie algorithm. As shown in the *Inset*, the differences ΔP between analytical results and stochastic simulations are of the order of 0.01. The excellent agreement validates our analytical approach, which ignores the stochastic nature of the growth and shrinkage processes. At $t \simeq 1,200$ s, the black line for the transition coupled to polymerization quickly approaches the asymptotic value $P(t = \infty) = 1$, because the simulated depolymerization process then reached the pointed end of the filaments. The parameter values used in these simulations are as follows: Duration of polymerization $t_{\text{pol}} = 300$ s, association rate $\omega_{\text{on}} = 21/\text{s}$, dissociation rate during elongation phase $\omega_{\text{off}}^{\text{el}} = 1/\text{s}$, dissociation rate during shrinkage phase $\omega_{\text{off}} = 5/\text{s}$. To match $\langle \tau \rangle \simeq 500$ s, we have chosen $Q = 4 \times 10^{-4}$ for the transition coupled to polymerization, $\omega = 4.375/\text{s}$ for the vectorial transition, and $\omega = 10^{-6}/\text{s}$ for the random transition.

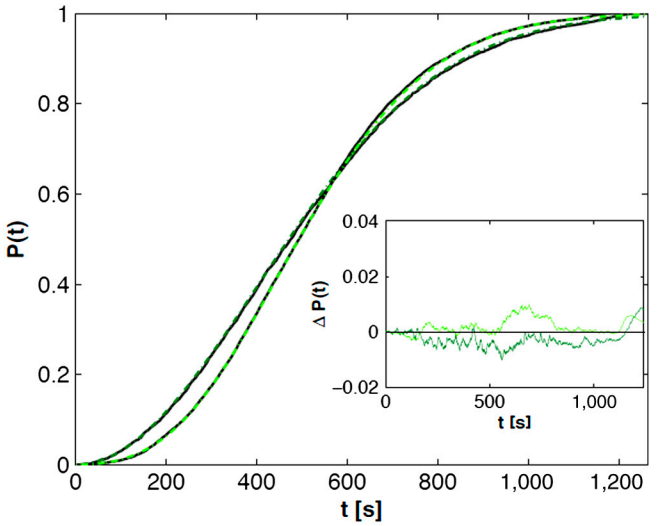

Fig. S2. Effect of hydrolysis on cumulative distribution function P. In the absence of hydrolysis, the cumulative distribution P versus time t is described by the dark green line, which is identical to the green line in Fig. S1. When the hydrolysis process is included in the theoretical analysis, the cumulative distribution P is determined by Eqs. **S11**–**S14**, which leads to the lime green line. The corresponding results from stochastic simulations lead to the continuous black lines. The inset displays the small differences Δ between the analytical results and the stochastic simulations, which demonstrates the excellent agreement between both computational methods and confirms the functional form of $P = P(t)$ as given by Eqs. **S11**–**S14**. Comparison of the dark green and the lime green lines shows that the presence of hydrolysis leads to relatively small changes in the cumulative distribution P. The parameter values corresponding to the dark green curve are identical to those in Fig. S1. The parameter values corresponding to the lime green curve are as follows: Duration of polymerization $t_{\text{pol}} = 300$ s, association rate of ATP-actin $\omega_{\text{on}} = 21/\text{s}$, dissociation rate of ATP-actin $\omega_{\text{off}}^{\text{T}} = 1/\text{s}$, effective depolymerization velocity $v_{\text{P}} = 1.5/\text{s}$ of ADP · P_i-actin, effective depolymerization velocity $v_{\text{D}} = 6.2/\text{s}$ of ADP-actin, cleavage rate $\omega_{\text{c}} = 0.3/\text{s}$, phosphate release rate $\omega_{\text{r}} = 0.007/\text{s}$, and transition rate $\omega = 10^{-6}/\text{s}$.

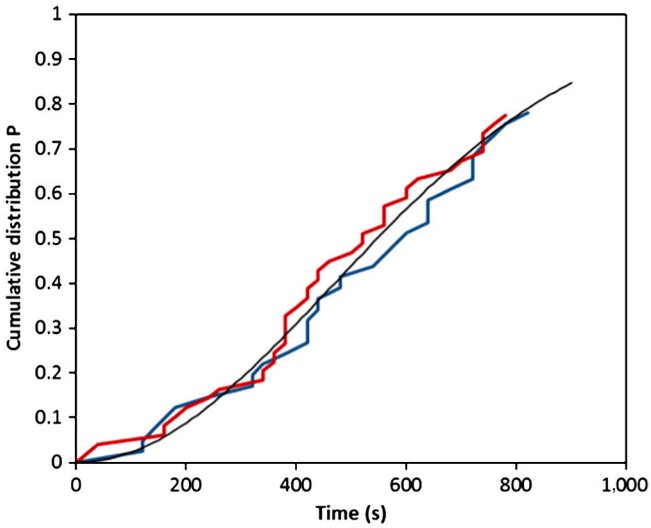

Fig. S3. The flow rate does not affect the statistics of interruptions. Cumulative distribution functions P versus time t for the occurrence of pauses as measured for Alexa488-labeled filaments depolymerizing in the presence of microfluidic flows: The blue and the red line correspond to a buffer flow rate of 5 μL/min and 25 μL/min, respectively. The black line is obtained from Eq. **1** with the protomer transition rate $\omega = 8 \times 10^{-7}$/s.

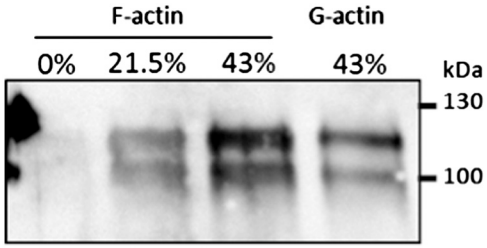

Fig. S4. Additional Western blots for solutions of Alexa488-labeled actin. The first three columns display Western blots for F-actin solutions with labeling fraction $X_{fl} = 0$, 0.215, and 0.43; the right column corresponds to G-actin solutions with labeling fraction $X_{fl} = 0.43$. The F-actin solutions had an actin concentration of 50 μM and were exposed to an illumination intensity of 0.04 mW/mm^2 for 1 h. The G-actin solution had an actin concentration of 52 μM and was exposed to the same illumination protocol. For the F-actin buffer, the dimer-to-monomer ratio ρ increases linearly with the labeling fraction X_{fl} according to $\rho \simeq 2.5 \times 10^{-3} X_{fl}$. For the G-actin buffer, the dimer-to-monomer ratio is $\rho \simeq 1.45 \times 10^{-3}$.

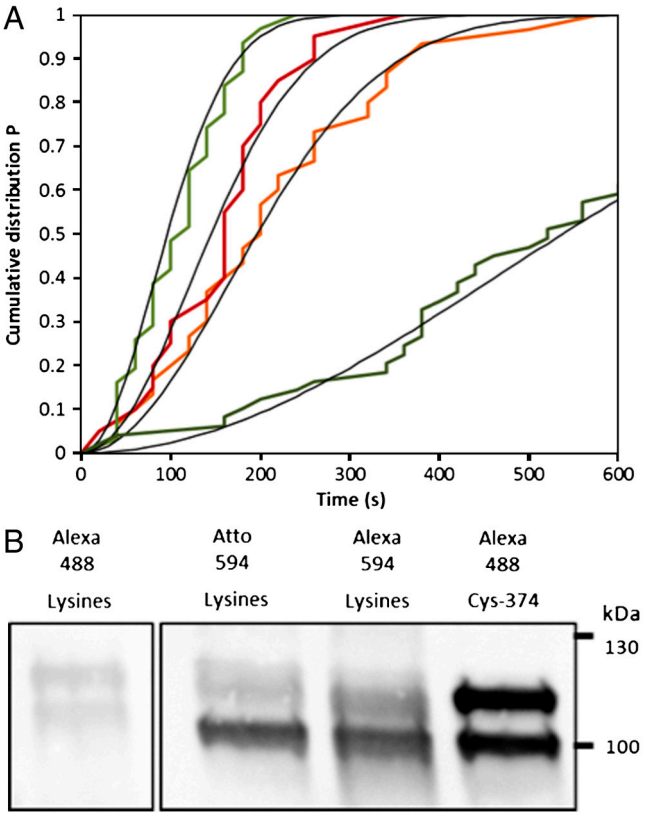

Fig. S5. Dimerization of F-actin for a variety of fluorophores. (*Top*) Cumulative distributions *P* versus time *t* for depolymerizing filaments containing 12% actin labeled on surface lysines with Alexa488 (dark green), Alexa594 (orange), Atto594 (red), and 15% actin labeled with Alexa488 on Cysteine-374 (light green). Judging from the lamp emission spectrum, illumination was three times stronger for Alexa594 and Atto594. Fitting the data to the theoretical curves (black lines) as obtained from Eq. **1** and taking differences in labeling fraction and illumination intensity into account, we estimate that labeling actin with Alexa594, Atto594, and Alexa488-Cys374, leads to a fivefold, ninefold, and 30-fold increase of the protomer transition rate ω, compared to labeling with Alexa488 on lysines. (*Bottom*) Western blots of the corresponding F-actin solutions directly confirm the formation of dimers for all four species of fluorescently labeled actin. The corresponding dimer-to-monomer ratios are consistent with the estimates obtained from the cumulative distributions *P*.

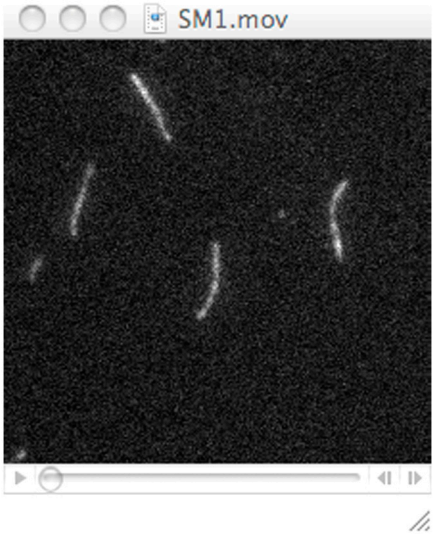

Movie S1. This movie corresponds to the setup in Fig. 1*A* (no flow): Top view of four actin filaments with their pointed ends attached to the coverslip surface. In the absence of additional attachment points, the filaments underwent pronounced bending undulations. The loss of these undulations implies that another filament segment became attached to the surface; one example is provided by the filament on the left that got stuck after about 140 s (real time corresponding to a lag time of 60 s and 2 s in the movie). Such filaments with suppressed bending undulations were not included in the analysis. The filament at the bottom became detached after about 460 s (corresponding to 10 s in the movie) and then diffused out of the field of view. Some additional filaments that were not attached to the surface also diffused in and out of the field of view. Observation with total internal reflection fluorescence microscopy ensured that the visible bending undulations occurred within the focal plane. The image width is about 40 μm. The movie is accelerated 40 ×.

Movie S1 (MOV)

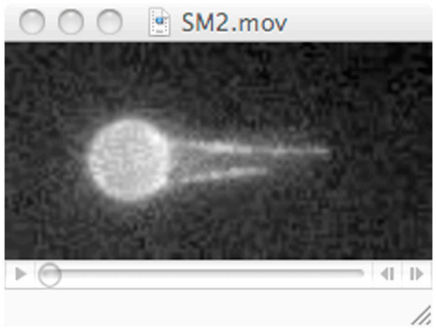

Movie S2. This movie corresponds to the setup in Fig. 1*B* (microfluidics flow): Actin filaments are depolymerizing from their barbed (right) ends, in buffer flowing from left to right. The filaments are anchored with their pointed (left) ends to a microbead via spectrin-actin seeds. Some filaments break up or detach from the surface and are then carried away by the buffer flow. The depolymerization of the longest filament is interrupted by a pause. The image width is 31 μm. The movie is accelerated 200 ×.

Movie S2 (MOV)

Movie S3. This movie corresponds to the setup in Fig. 1*C* (microfluidics flow): Actin filaments are depolymerizing from their barbed (right) ends in buffer flowing from left to right. The filaments are anchored with their pointed (left) ends to the coverslip surface via spectrin-actin seeds. Some filaments depolymerize completely, while the depolymerization of other filaments is interrupted by a pause. A few filaments break up or detach from the surface, and are then moved out of the field of view. The image width is 53 μm. The movie is accelerated 160 ×.

Movie S3 (MOV)

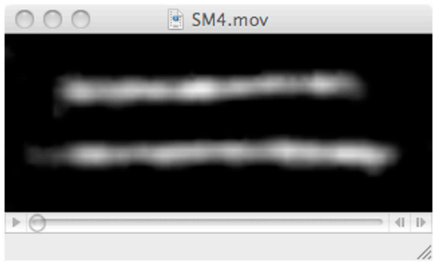

Movie S4. Direct visual inspection can distinguish "intrinsic pauses" caused by actin dimerization from "extrinsic" pauses arising from additional surface attachments: Two actin filaments, which are attached at their pointed (left) ends to the coverslip surface via spectrin-actin seeds, are depolymerizing from their barbed (right) ends, in buffer flowing from left to right. After 900 s (real time corresponding to 3 s in the movie), the depolymerization of the upper filament is interrupted when its barbed end sticks to the surface, whereas the lower filament pauses without sticking to the surface as one can conclude from the thermal fluctuations of the barbed ends: these fluctuations are suppressed for the upper filament but remain clearly visible for the lower filament. The image width is 19 μm. The movie is accelerated 300 ×.

Movie S4 (MOV)

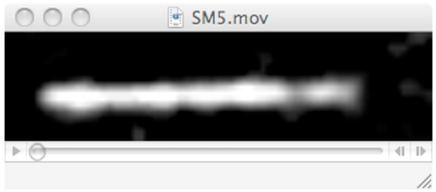

Movie S5. Two subsequent interruptions of an actin filament at the same filament position: Initially, the filament is depolymerizing from its barbed (right) end, in buffer flowing from left to right. The depolymerization process is interrupted by a pause: The red mark indicates the position of the barbed end during the first pause. The filament is then reelongated for 2 min by flowing in G-actin. The elongation process is not shown but the yellow mark indicates the position of the barbed end after elongation. A second depolymerization process is initiated by flowing in buffer again. This second depolymerization process is again interrupted when the barbed end reaches the red mark. The image width is 18 μm. The movie is accelerated 160 ×.

Movie S5 (MOV)